Synthesis and Thermal Treatment of Hydroxyapatite Doped with Magnesium, Zinc and Silicon

FIRUTA GOGA[1], EDIT FORIZS[1]*, ALEXANDRA AVRAM[1], ADELA ROTARU[1], ANAMARIA LUCIAN[1], IOAN PETEAN[1], AURORA MOCANU[1], MARIA TOMOAIA COTISEL[1,2]*

[1]Babes-Bolyai University of Cluj-Napoca, Faculty of Chemistry and Chemical Engineering, Physical Chemistry Centre, 11 Arany Janos Str., 400084, Cluj Napoca, Romania

[2]Academy of Romanian Scientists, 54 Splaiul Independentei, 050094, Bucharest, Romania

Pure nano-crystalline hydroxyapatite (Hap) and Hap doped with magnesium, zinc and silicon, namely Hap-0.25wt%Mg: Hap01, Hap-0.25wt%Mg-0.47wt%Si: Hap02, Hap-1.50wt%Mg-0.47wt%Si: Hap03, Hap-0.67wt%Mg-0.2wt%Zn-0.13wt%Si: Hap04, were synthesized using aqueous precipitation method. The pure and doped Hap were calcined individually at 400, 650 and 850 °C for 2h, and investigated by Brunauer-Emmett-Teller (BET) specific surface area and porosity measurements, as well as by X-ray powder diffraction (XRD). The morphology and particle size of nano-crystalline powders were investigated using scanning electron microscopy (SEM) and atomic force microscopy (AFM). The thermal stability of the obtained nanoceramics from 30°C to 1000°C and the effect of calcination temperatures (400, 650 and 850 °C) on their composition and structure were also determined by using TG, DTG, TGA and DTA techniques coupled with SEM-EDX. Results analysis shows a high thermal stability (up to 1000 °C) of these nanomaterials, including the triple-substituted Hap with Mg, Zn and Si (Hap04). Simultaneous incorporation of Mg, Zn and Si into Hap lattice represents a novelty and promotes a new generation of synthetic porous nanoceramics with unique Hap structure, and high thermal stability. Due to their chemical composition and structure rather similar to those characteristic for the inorganic component of bone, these nanoceramics can have multiple applications in biomedicine, as bone substitutes, for metal coatings and in drug delivery systems.

Key words: nanoceramics, doped hydroxyapatite, magnesium, zinc, silicon

Hydroxyapatite, $Ca_{10}(PO_4)_6(OH)_2$: Hap, due to its similarity with inorganic component from human bones and teeth has been extensively studied as a biocompatible and bioactive material [1-3]. Accordingly, Hap nanoparticles can significantly increase the biocompatibility and bioactivity of various artificial biomaterials. Over the past decade the preparation of synthetic Hap nanoparticles has been intensively investigated to develop new synthetic routes. At the same time important efforts have been made for enhancing the bioactivity and mechanical properties of hydroxyapatite. The bioactivity can be improved by incorporating ionic constituents in Hap structure (SiO_4^{2-} and CO_3^{2-} for phosphate, Mg^{2+}, Zn^{2+}, Na^+, K^+ for Ca^{2+}) [4], because it is proven that the hydroxyapatite rather easily accepts ions in its crystalline lattice. Over the past years, several ceramics have been prepared through doping hydroxyapatite with F^-, CO_3^{2-}, Na^+, Mg^{2+}, Mn^{2+}, Zn^{2+}, but most of them being primarily mono substituted Hap. Through elemental substitution within the Hap structure various advantages are encountered. For example, silicon is important in the calcifying process of bones, and in consequence, bioceramics based on Hap doped with silicon are intensely studied for their bioactivity [5-7]. Further, the adsorbed –Si-OH groups at the Hap nanoparticle surface can modulate the nucleation and the crystallite growth [8, 9] leading to the controlled formation of nanosized Hap particles.

Since Mg^{2+} and CO_3^{2-} are components of natural bone, bioceramics containing these ions are entitled to have superior characteristics to pure Hap [10]. Furthermore, magnesium is known to influence both bone matrix and bone mineral metabolism. As the magnesium content of bone mineral decreases, bone crystals become larger and more brittle. Thus, the effect of magnesium as a dopant on hydroxyapatite characteristics is a subject of numerous studies [11, 12]. Magnesium doped hydroxyapatites ($Ca_{10-x}Mg_x(PO_4)_6OH_2$) are appropriate as biomaterials, because Mg^{2+} in Hap structure has an adsorbent role at the surface of particles and contributes to the binding of bioceramics to organic substances in that system [13-15]. Several techniques can be mentioned for the synthesis of magnesium doped hydroxyapatites: aqueous precipitations [16-18], sol-gel technique [19, 20], solid-state reactions [21], microwave-assisted synthesis [22], and hydrothermal synthesis [23]. Mg and Si co-doped hydroxyapatite is also of great interest because it may be applicable as artificial bone [23-25]. Zn is another important constituent of bone tissues, being involved in bone regeneration and in cellular growth and proliferation [26-28].

Due to an augmented demand for synthetic hydroxyapatites, possessing closer characteristics to biological Hap [29], the interest in safe production of multi-substituted Hap [30-33] is justified and recently highly increased [34-36]. Therefore, an important objective is arising to develop multi-substituted Hap with high thermal stability and enhanced physical, chemical, mechanical and biological properties. To reach this goal, the modification in chemical composition is an excellent approach in tailoring the properties of synthetic hydroxyapatites but involves many challenges. Evidently, the controlled reaction conditions, such as *p*H and temperature, followed by the aging time at selected temperatures [6, 30, 36], and the right choice of thermal treatment parameters are essential [16, 29] and play a major role in realization of these bioceramics based on hydroxyapatites with appropriate composition for biomedical applications.

---

* email: eforizs@chem.ubbcluj.ro; mcotisel@gmail.com

Although there are studies in this field, a systematic characterisation of doped Hap with Mg, Zn and Si, synthesized under identical experimental conditions has not been reported. Here we report a simple aqueous precipitation method for the preparation of pure hydroxyapatite and hydroxyapatite doped with a various content of magnesium, zinc, and silicon, used separately and combined. The significant influence of the preparation methodology and thermal treatment approach on the features of multi-substituted Hap is evidenced in this work for various hydroxyapatites, doped with Mg, Zn and Si, and it is also documented for the fabrication of various other compounds [37-39].

The resulting nanoceramic powders were investigated by thermogravimetric analysis (TGA) and differential thermal analysis (DTA) as well as by Brunauer-Emmett-Teller (BET) specific surface area and porosity measurements. The surface morphology was analysed by scanning electron microscopy (SEM) and atomic force microscopy (AFM). The phase analysis and the chemical composition were performed by X-ray diffraction (XRD) and elemental analysis by energy-dispersive X-ray spectroscopy (EDX).

Experimental part

Materials and methods

The following compounds $Ca(NO_3)_2 \cdot 4H_2O$, $(NH_4)_2HPO_4$, $Mg(NO_3)_2 \cdot 6H_2O$, $Zn(NO_3)_2 \cdot 6H_2O$, tetraethyl orthosilicate ($(C_2H_5O)_4Si$, TEOS) and chlorotrimethyl silane ($(CH_3)_3SiCl$, TMS) were used as starting materials, as Ca, P, Mg, Zn and Si precursors. Pure stoichiometric Hap and four doped hydroxyapatites with different content of Mg, Zn and Si (table 1) were prepared using a wet precipitation method, developed previously by us [6, 26, 27, 33]. All chemicals were reagent grade and purchased form Merck and Sigma-Aldrich. All solutions were prepared with deionized water.

Synthesis of pure Hap and doped Hap

The pure stoichiometric hydroxyapatite was prepared, as a control, with the starting Ca/P molar ratio equal to the stoichiometric value of 1.67. Similarly, the simultaneous doping of the synthetic hydroxyapatite with Mg, Zn and Si was performed including the appropriate amount of each element in the synthesis in alkaline solution.

As a general procedure, aqueous $Ca(NO_3)_2$ solutions without or with an appropriate amount of $Mg(NO_3)_2$ (Hap01-Hap04) and $Zn(NO_3)_2$ (Hap04), was added at 70 °C, under vigorous stirring (800 rpm) to an aqueous $(NH_4)_2HPO_4$ solution of suitable concentration corresponding to Ca/P molar ratio of 1.67 (for pure stoichiometric Hap), or containing the calculated amount of Si for each sample (Hap02-Hap04, Table 1), added as TMS (Hap02) or TEOS (Hap03-Hap04). The nonylphenol, $C_{15}H_{24}O$, was added in 0.1 % proportion relative to final product to control the crystal growth of Hap or doped Hap. The pH of the reaction mixture was adjusted at 11.5-12 with concentrated aqueous ammonia, 25%, in the presence of ethylene-diamine (1,2-ethanediamine, EDA). The reaction parameters for the synthesis of pure Hap and doped Hap were identical. The maturation of the resulting dispersion was conducted at 70 °C, for 24 h in reactor, under moderate stirring for the formation of nanocrystalline product. The obtained suspension was filtered. The precipitate was carefully washed with deionised water until free of NO_3^- ions, and the resulted materials were dried by lyophilisation. The dried materials (pure stoichiometric Hap and Hap01-Hap04) were each calcined separately at 400°C (2 h), 650°C (2 h), or 850°C (2 h).

Characterisation methods

Thermal behaviour of pure Hap and doped Hap powders was determined by thermogravimetric analysis (TGA) and differential thermal analysis (DTA), for the temperature range from 30 to 1000 °C, using Universal SDTQ600 TA Instruments. Samples were heated in alumina crucibles at a constant heating rate of 10 °C/min, in flowing air, using simultaneous TG/DTG-DTA techniques.

BET specific surface area, pore volume and pore size distribution were determined for Hap powders with an automated Sorptomatic 1990 instrument, with nitrogen adsorption at 77 K. The calculation of surface area was made in the P/Po range between 0.03 and 0.3, and the total pore volume was determined at P/Po = 0.95. Before BET measurements the samples were outgassed [27] for 6 h at 70°C.

X-Ray diffraction (XRD) investigations were carried out using a Bruker D8 Advance diffractometer, in Bragg-Brentano geometry, equipped with a X-ray tube with copper K_{α} line, wavelength 1.541874 Å). Phases were identified by comparing the peak positions of the diffraction patterns with PDF files.

All samples were imaged by scanning electron microscope: SEM, JEOL 5600 LV, using backscattered-electron (BSE) and secondary electron imaging (SEI) techniques [6]. The SEM samples were deposited as a uniform layer on the adhesive graphitized tape and were examined in low vacuum (23 Pa), with an accelerating voltage of 15 kV, a working distance of 20 mm, at 1000 to 30,000 magnifications. For local elemental analysis of different samples, the energy-dispersive X-ray (EDX) spectroscopy was used coupled with SEM imaging.

Atomic force microscopy imaging was obtained using JEOL 4210 AFM equipment, operated in tapping mode [40, 41], with standard cantilevers with silicon nitride tips (resonant frequency in the range of 200–300 kHz). The sample layer was deposited on glass support. Different areas from $10\mu m \times 10\mu m$ to $0.5\mu m \times 0.5\mu m$ were scanned on the same layer. The AFM images and cross-section profiles along a selected direction were processed by the standard procedures.

Results and discussions

The syntheses for Ca substitution with Mg into hydroxyapatite (Hap) lattice are based on the reaction:

$$(10-x)Ca(NO_3)_2 + xMg(NO_3)_2 + 6(NH_4)_2HPO_4 + 8NH_4OH \longrightarrow \\ Ca_{10-x}Mg_x(PO_4)_6(OH)_2 + 20NH_4NO_3 + 6H_2O$$

where, x has values from 0 to 10, as seen in table 1 from theoretical formula for stoichiometric Hap. For Ca substitution with Mg and Zn simultaneously, the $(Ca^{2+} + Mg^{2+} + Zn^{2+})/PO_4^{3-}$ ratio was maintained 1.667 for all samples, which is the stoichiometric value for Hap structure. The element content is given in weight % (wt%) and in the moles of element/ mole Hap, also shown in Table 1, for the synthesized Hap powders.

The substitution of PO_4^{3-} and OH^- with SiO_4^{4-} is also possible simultaneously with cationic substitution and gives $Ca_{10-x}Mg_x(PO_4)_{6-z}(OH)_{2-z}(SiO_4)_z$ for the Hap doped with Mg and Si. The formula for a tri-substituted Hap with Mg, Zn and Si is: $Ca_{10-x-y}Mg_x Zn_y (PO_4)_{6-z}(OH)_{2-z}(SiO_4)_z$.

Thus, synthesized Hap products in this work have general formula $Ca_{10-x-y}Mg_xZn_y(PO_4)_{6-z}(OH)_{2-z}(SiO_4)_z$, that for x = y = z = 0 corresponds to pure stoichiometric hydroxyapatite, Hap: $Ca_{10}(PO_4)_6(OH)_2$.

The dopants play an important role in the bone cells response. For example, Mg^{2+} and Zn^{2+} ions are linked to an

Table 1

COMPOSITIONS OF SYNTHESISED HYDROXYAPATITES DOPED WITH Mg, Zn AND Si (Hap-Mg-Zn-Si)

Doped Hap nanopowders			Wt%	Moles of element/ mole Hap	Formula
	Sample Code	Element			
Hap-0.25%Mg	Hap01	Ca	39.7	9.90	$Ca_{9.90}Mg_{0.10}(PO_4)_6(OH)_2$
		Mg	0.25	0.10	
		Zn	0	0	
		Si	0	0	
		P	18.6	6	
Hap -0.25%Mg-0.47% Si	Hap02	Ca	39.7	9.90	$Ca_{9.90}Mg_{0.10}(PO_4)_{5.83}(SiO_4)_{0.17}(OH)_{1.83}$
		Mg	0.25	0.10	
		Zn	0	0	
		Si	0.47	0.17	
		P	18.1	5.83	
Hap -1.50%Mg - 0.47% Si	Hap03	Ca	38.0	9.39	$Ca_{9.39}Mg_{0.61}(PO_4)_{5.83}(SiO_4)_{0.17}(OH)_{1.83}$
		Mg	1.50	0.61	
		Zn	0	0	
		Si	0.47	0.17	
		P	18.2	5.83	
Hap -0.67%Mg-0.2%Zn-0.13% Si	Hap04	Ca	38.8	9.69	$Ca_{9.69}Mg_{0.28}Zn_{0.03}(PO_4)_{5.95}(SiO_4)_{0.05}(OH)_{1.95}$
		Mg	0.67	0.28	
		Zn	0.20	0.03	
		Si	0.13	0.05	
		P	18.4	5.95	

enhanced activity of osteoblasts [26, 36] and their presence as dopants within Hap structure can enhance Hap bioactivity. Silicon is also important in bone metabolism and has beneficial effect on the biological response of osteoblasts, as reported recently elsewhere [6]. The doping of Hap with various elements, such as Mg, Zn and Si, might influence thermal stability, crystal structure, morphology and porosity of the resulting doped Hap powders.

Thermal behaviour

Thermal behaviour of the four synthesised doped Hap powders, Hap01-Hap04 (table 1), previously calcined at 400 °C, is compared with that corresponding to non-calcined pure Hap (Hap-nc) and calcined Hap (Hap-c) at 400 °C. Thermal analysis (TGA/DTA) was performed on all samples in the temperature range of 30-1000°C. Thermogravimetric (TG) curves and difference in temperature (DT), between sample and reference, curves are given in figure1 for all six investigated powders. A summary of the weight loss (Δm) as well as the residue weight is given in table 2, determined by TGA, for specific temperature ranges obtained for pure Hap-nc and Hap-c, as well as for doped Hap samples: Hap01-Hap04.

The average weight loss for non-calcined pure Hap, Hap-nc, recorded by TGA for 30-1000°C was 9.51% (table 2) due to a relatively high content of water. In comparison Hap-c showed a weight loss of only 6.65% which can be primarily attributed to a relatively low content of water existing within as obtained Hap-c (pure Hap previously calcined at 400°C). The smallest average weight loss recorded for Hap01 (5.21%) and Hap02 (5.02%) might be correlated with a lower amount of water within these doped Hap powders and only slightly lower than for Hap-c. The Hap03 and Hap04 exhibited a weight loss of 6.94% and 6.30%, respectively, which is around 6.65% found for pure Hap-c. These findings support a high thermal stability of doped Hap powders with Mg, Zn and Si.

The corresponding DTA data revealed an endothermic process for all samples. DTA analysis (fig.1) of Hap-nc, Hap-c, Hap01-Hap04 are in substantial agreement with XRD results, indicating a good structure stability of these powders. The endothermic effect observed in temperature range between 50 and 150 °C for all powders is due to the removal of physically adsorbed water and CO_2 in agreement with other reported data [17] for mono substituted Hap. Then, the weight loss up to 620 °C might be caused at least partially by the decomposition of organic reagents used in synthesis of Hap, as reported for biological Hap [29].

Analysing the data in figure 1 and the weight loss in table 2, some details of thermal behaviour can be further discussed. The gradual loss in weight for Hap-nc (8.65% for heating up to 760°C, a) is higher than for Hap-c (5.38% for heating up to 758°C, b), which is slightly higher than for Hap01 (4.28% for heating up to 797°C, c), which is equal to that for Hap02 (4.22% for heating up to 677°C, d), which is smaller than for Hap04 (5.32% for heating up to 713°C, f), which is smaller than for Hap03 (6.03% for heating up to 747°C,e). The weight loss and the corresponding endotherms might be explained by the gradual loss of water from hydration layers, surrounding individual particles and aggregated particles, as well as from water adsorbed on the surface of Hap particles [14, 16], including lattice water (e.g., coordinated water molecules with surface ions) from these nano powders, in substantial agreement with reported data on mono-substituted Hap with Mg or Zn [36]. At heating up from noted high temperatures (table 2) to 1000°C, the weight loss is about 0.86% for Hap-nc, which is not far from 0.93% recorded for Hap01, and rather close to 0.80% for Hap02, and near to 0.91% for Hap03 and rather close to 0.98% for Hap04 and only slightly smaller than 1.27%, recorded for Hap-c. This small weight loss about 1% found for these powders might be attributed to the decomposition of possible $CaCO_3$ traces [18], due to the nano powder synthesis in air, and/or to the loss of lattice water [36]. Nevertheless, the structural dehydroxylation of Hap and doped Hap powders cannot be ruled out [29] at very high temperature close to 1000°C.

Certainly, the smaller nano particles (measured from AFM images) and their porous aggregates, illustrated in SEM images, indicate larger surface areas, which may explain the higher adsorption of surface water, particularly for Hap03 and Hap04 powders, in substantial agreement with BET analysis (table 3), calcined especially at 400 and 650 °C.

These results revealed also the importance of the structure of water on the surface of Hap and doped Hap

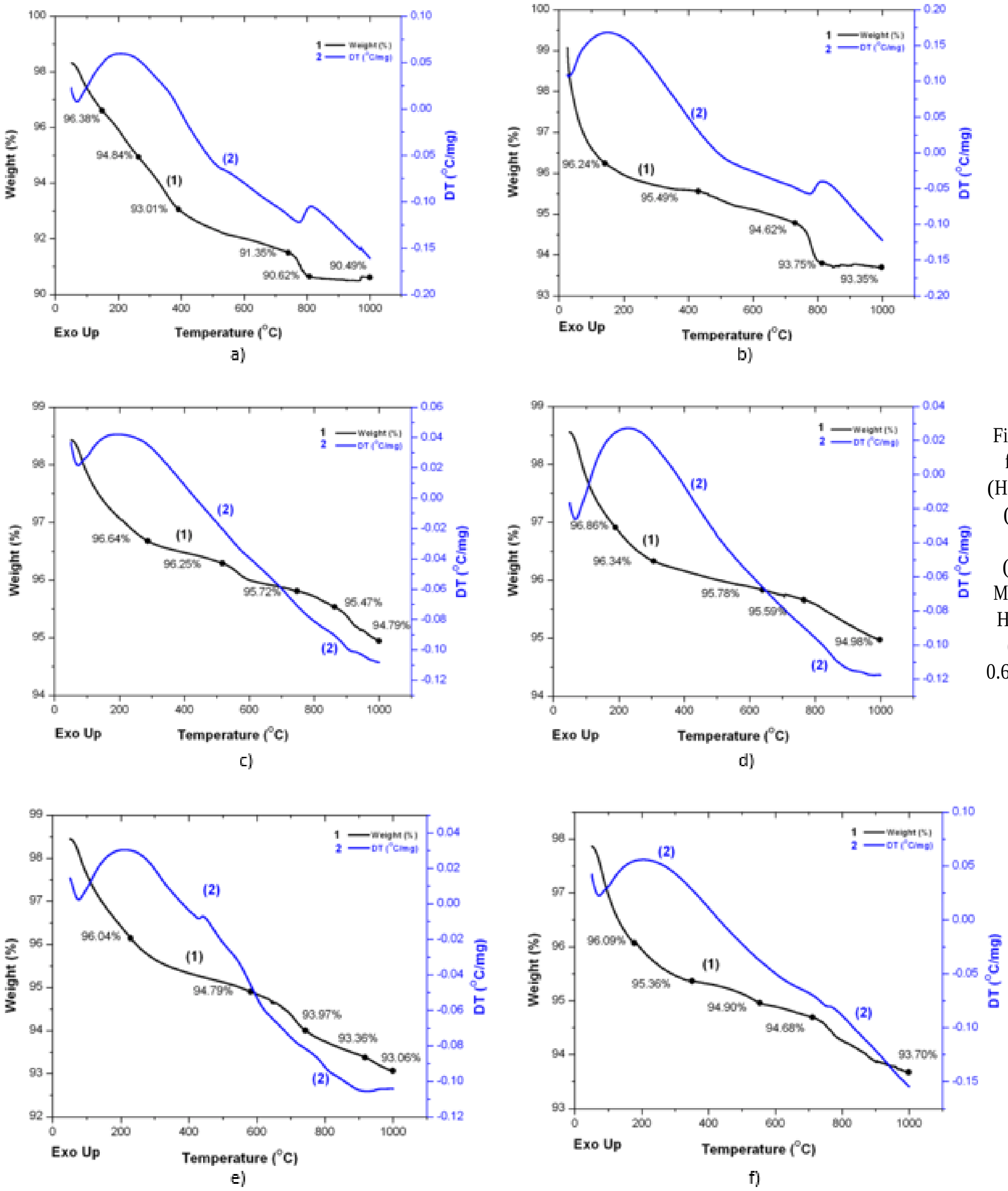

Fig. 1. TG and DT curves for non-calcined Hap (Hap-nc, a), calcined Hap (Hap-c, b) and doped Hap: Hap-0.25% Mg (Hap01, c); Hap-0.25% Mg- 0.47% Si (Hap02, d); Hap-1.50% Mg- 0.47% Si (Hap03, e); and Hap-0.67% Mg-0.2%Zn-0.13% Si (Hap04, f)

Table 2

WEIGHT LOSS (Δm) DETERMINED BY TGA FOR PURE HAP (Hap-nc AND Hap-c) AND Hap POWDERS DOPED WITH Mg (Hap01), OR DOPED WITH Mg AND Si (Hap02 AND Hap03) AS WELL AS DOPED WITH Mg, Zn AND Si (Hap04), ALL DESCRIBED IN TABLE 1

Powders	Sample Code	Temperature °C	Δm %	Residue %
Hap non-calcined	Hap-nc	30-760	8.65	
		760-1000	0.86	
		30 - 1000	9.51	90.49
Hap calcined	Hap-c	30-758	5.38	
		758-1000	1.27	
		30 - 1000	6.65	93.35
Hap-0.25% Mg	Hap01	30-797	4.28	
		797-1000	0.93	
		30 - 1000	5.21	94.79
Hap-0.25% Mg- 0.47% Si	Hap02	30 -677	4.22	
		677-1000	0.80	
		30 - 1000	5.02	94.98
Hap-1.50% Mg- 0.47% Si	Hap03	30-747	6.03	
		747-1000	0.91	
		30 - 1000	6.94	93.06
Hap-0.67% Mg-0.2%Zn-0.13% Si	Hap04	230- 713	5.32	
		713-1000	0.98	
		30 - 1000	6.30	93.70

Table 3
BET SPECIFIC SURFACE AREA (SSA) OF HAP DOPED WITH Mg, Zn AND Si, CALCINED POWDERS AT THREE CALCINATION TEMPERATURES: 400, 650 OR 850°C; EACH POWDER INDEPENDENTLY CALCINED FOR 2h

Powders	Sample Code	SSA, m^2/g		
		400 (°C)	650 (°C)	850 (°C)
Hap-0.25% Mg	Hap01	81	52	48
Hap-0.25% Mg- 0.47% Si	Hap02	95	57	11
Hap-1.50% Mg- 0.47% Si	Hap03	110	84	9
Hap-0.67% Mg-0.20%Zn-0.13% Si	Hap04	105	54	19

nanoparticles. Generally, the size, shape and surface chemical composition of nanoparticles affect the surface water layers. These findings are in substantial agreement with the data found on hydrated magnesium oxide nanoparticles by using molecular dynamics simulations [42], emphasizing that the extent of water hydration (i.e., highly ordered layers) and the water coordination number depend strongly on the nanoparticle characteristics. Undoubtedly, the water structure on the surface of nanoparticles is involved in different surface processes with impact on crystal growth and dissolution.

BET analyses

The specific surface area, SSA, and porosity have an important role concerning the behaviour of bioceramics based on Hap in various biomedical applications. A good biocompatibility is characterised by a large SSA and high porosity of bioceramics. In this respect, the choice of calcination temperature is crucial because it might correspond to major transformations that could take part in that bioceramic structure and consequently to modify its properties. Certainly, thermal stability of bioceramics needs first to be evaluated particularly for safe Hap sintering and Hap coatings on metal.

The results of Brunauer-Emmett-Teller (BET) analysis, in terms of SSA values and pore volume in doped Hap powders, show the importance of their chemical composition, calcined temperatures and the time allowed for calcination. In the following, SSA values are given in table 3, for Hap powders doped with Mg, Zn and Si, calcined at three different temperatures, namely, at 400, 650 and 850°C with a plateau of 2 h, each.

As a general effect, the SSA decreases with the increasing of calcination temperatures for a particular chemical composition in doped Hap (table 3). The influence of calcined temperature is higher in the case of Hap02 and Hap03, with the largest content of silicon, and also for Hap04, doped simultaneously with Mg, Zn and Si.

As a consequence of calcination from 400 to 850°C, the SSA for Hap01, Hap-0.25% Mg, decreased from 81 m^2/g to 48 m^2/g, respectively as given in table 3. In the case of Hap02, Hap-0.25% Mg-0.47%Si, the decrease in SSA was from 95 m^2/g found at 400 °C to 11 m^2/g found at 850 °C. In the case of Hap03, Hap-1.50 % Mg-0.47%Si, with a significant increased content in Mg, but the same Si content as in Hap02, the effect on SSA at calcination, namely from 110 m^2/g, at 400°C to 9 m^2/g at 850°C is significantly increased than for Hap02. For Hap04, Hap-0.67%Mg-0.2%Zn-0.13%Si, the effect of calcination on SSA is much higher than for Hap01. Thus, the gradual decrease of SSA with the increasing in calcination temperatures is dependent on the dopant amount and on the multiple substitutions within Hap lattice.

The significant effect on SSA is obtained for Hap doped with Si for the same quantity in Mg (0.25%), when Hap02 is compared with Hap01, and particularly at the highest calcination temperature of 850°C (table 3). Moreover, for the high content in Mg (e.g., six times bigger in Hap03 than in Hap02), the SSA is almost the same, at 850°C, for both powders. It appears rational to establish that a significant effect is brought by the Si content in these Hap02 and Hap03 powders, in comparison with Hap01 powder, at the highest calcination temperature. For triple substituted Hap04 with small quantities of Mg, Zn and Si, the SSA is affected but in a smaller degree than for Hap03, showing the importance of cations and anions simultaneously incorporated within the Hap lattice.

Also, a progressive decrease in the pore volume was observed during calcination, for every doped Hap powder, Hap01-Hap04, calcined individually at 400, 650 or 850 °C. For instance, Hap01 showed a total decrease of pore volume, from about 0.13 cm^3/g to 0.06 cm^3/g; Hap02 showed a decrease from about 0.20 cm^3/g to 0.01 cm^3/g; Hap03 showed a decrease from 0.19 cm^3/g to 0.01 cm^3/g; and Hap04 showed a decrease of pore volume, from 0.18 cm^3/g to 0.02 cm^3/g. This finding can be explained by a possible crash of large pores within Hap lattice during the calcination process, which is somehow facilitated by the presence of Si in the HAP lattice.

Structural XRD analyses

The effect of calcination temperature on powders was also studied using XRD analyses for all samples. Several representative examples of XRD patterns are given for Hap01 powder, calcined at 650°C (fig. 2a) and 850 °C (fig. 2b), as well as for Hap03 powder, and calcined at the same temperatures (fig. 2c and fig. 2d). The diffraction peaks match well with those of the stoichiometric Hap phase (09-0432 PDF), suggesting that Hap is the unique phase present in all samples.

All samples, calcined at 400°C or at 650°C, are formed from nanocrystalline particles as revealed by AFM images (fig. 5) while increasing calcined temperature to 850°C, a porous aggregated crystalline structure is visualized by SEM images, (figs. 3 and 4).

Morphological studies

As an example of representative SEM micrographs, figure 3 shows the morphology of powders: Hap01: $Ca_{9.90}Mg_{0.10}(PO_4)_6(OH)_2$ (a, b) and Hap04: $Ca_{9.69}Mg_{0.28}Zn_{0.03}(PO_4)_{5.95}(SiO_4)_{0.05}(OH)_{1.95}$ (c, d). SEM micrographs indicate that the particles of Hap01, calcined at 850°C (fig. 3b), are more aggregated than in Hap01 powder, calcined at lower temperature of 650°C (fig. 3a). A porous aggregated structure is also revealed by figures 3c and 3d for Hap04, calcined at 850 °C. Further, SEM image (fig. 3c) illustrates different aggregates for Hap04 than for Hap01 (fig. 3b), although both powders were calcined at the same temperature of 850°C. The difference in morphology can be related to the chemical composition of Hap04 doped with Mg, Zn and Si against Hap01, which contains only a small quantity of Mg. Certainly, this behaviour represents a

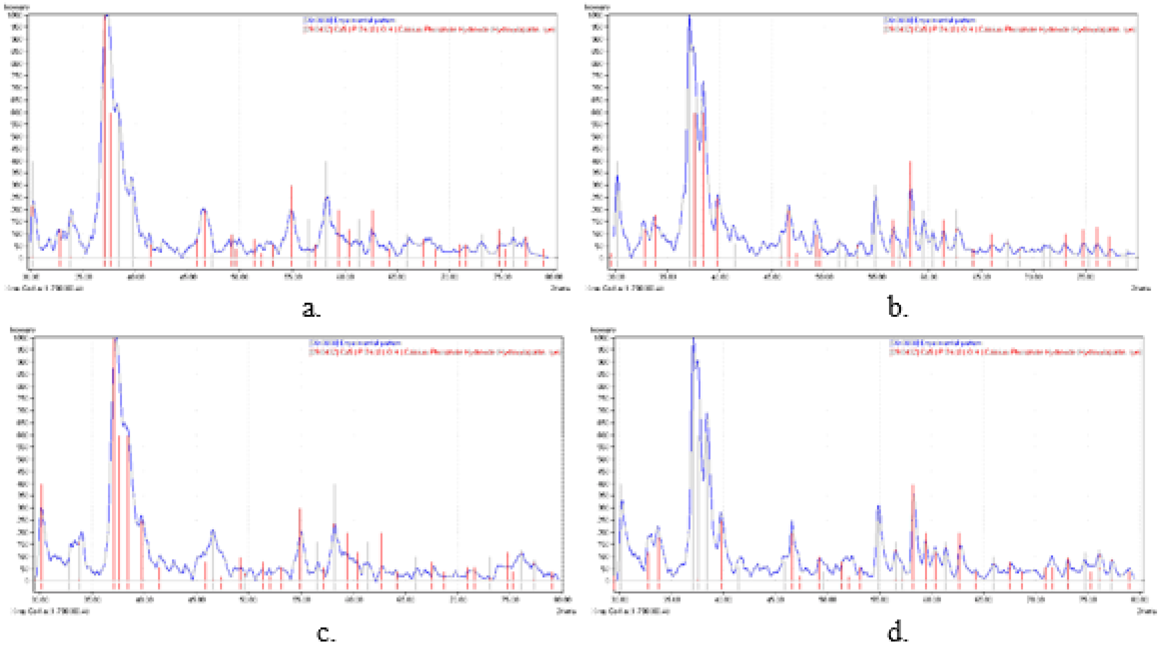

Fig. 2. XRD patterns for Hap01: $Ca_{9.90}Mg_{0.10}(PO_4)_6(OH)_2$ (a, b) and Hap03: $Ca_{9.39}Mg_{0.61}(PO_4)_{5.83}(SiO_4)_{0.17}(OH)_{1.83}$ (c, d); calcined at 650°C (a, c) and 850°C (b, d); compared with PDF 09-0432 for pure stoichiometric hydroxyapatite

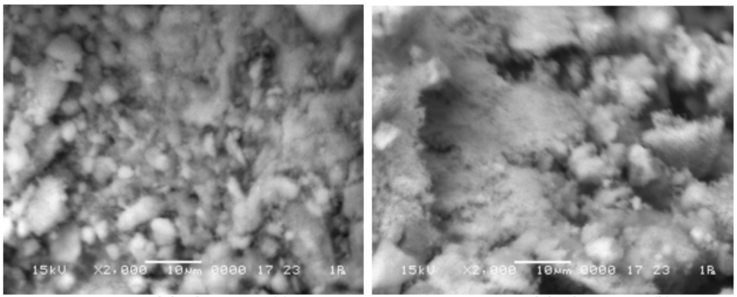

Hap01, calcined at 650 °C (a) Hap01, calcined at 850 °C (b)

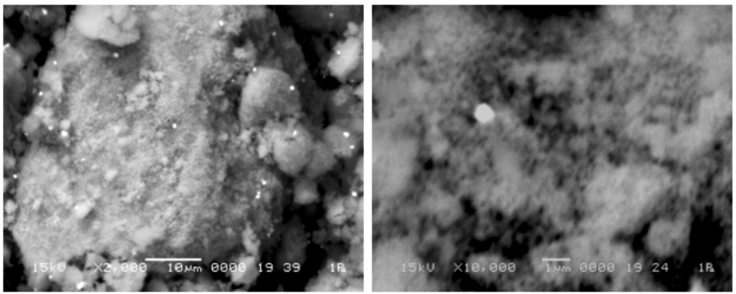

Hap04, calcined at 850 °C (c) Hap04, calcined at 850 °C (d)

Fig. 3. SEM images for Hap01: $Ca_{9.90}Mg_{0.10}(PO_4)_6(OH)_2$, powder calcined at 650 °C (a) and 850 °C (b); and Hap04: $Ca_{9.69}Mg_{0.28}Zn_{0.03}(PO_4)_{5.95}(SiO_4)_{0.05}(OH)_{1.95}$ (c, d), powder calcined at 850°C. Bars in SEM images: of 10µm (a, b, c) and 1 µm (d)

general characteristic for all doped Hap (Hap01-Hap04) powders.

Moreover, SEM results are in substantial agreement with BET measurements (table 3). Therefore, the specific surface area for Hap04 calcined at 850°C (19 m²/g) is much smaller than for Hap01 (48 m²/g). Through calcination of Hap04, the pore volume decreased from about 0.18 cm³/g, found at 400°C, to about 0.02 cm³/g, at 850°C, and in consequence, the specific surface area gradually decreased and the particle size increased. A similar situation is encountered for all samples.

The thermal treatment of doped Hap powders produced insignificant changes in XRD patterns. Accordingly, a unique Hap structure is identified for all investigated samples, indicating a good thermal stability of these powders as found by TGA and DTA data (fig. 1, table 2).

The elemental analysis of Hap01-Hap04 powders was determined by SEM-EDX technique. The EDX analysis showed the presence of Ca, P, Mg and O in all powders,

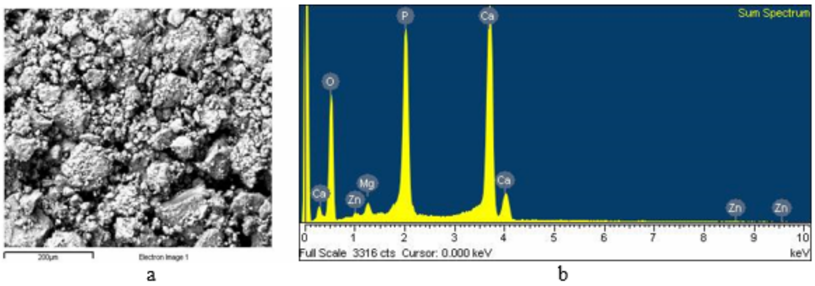

Fig. 4. SEM image for the Hap04, $Ca_{9.69}Mg_{0.28}Zn_{0.03}(PO_4)_{5.95}(SiO_4)_{0.05}(OH)_{1.95}$ calcined at 650°C (a) and results of the EDX analysis; the amount of Ca, P, O, Mg and Zn is revealed

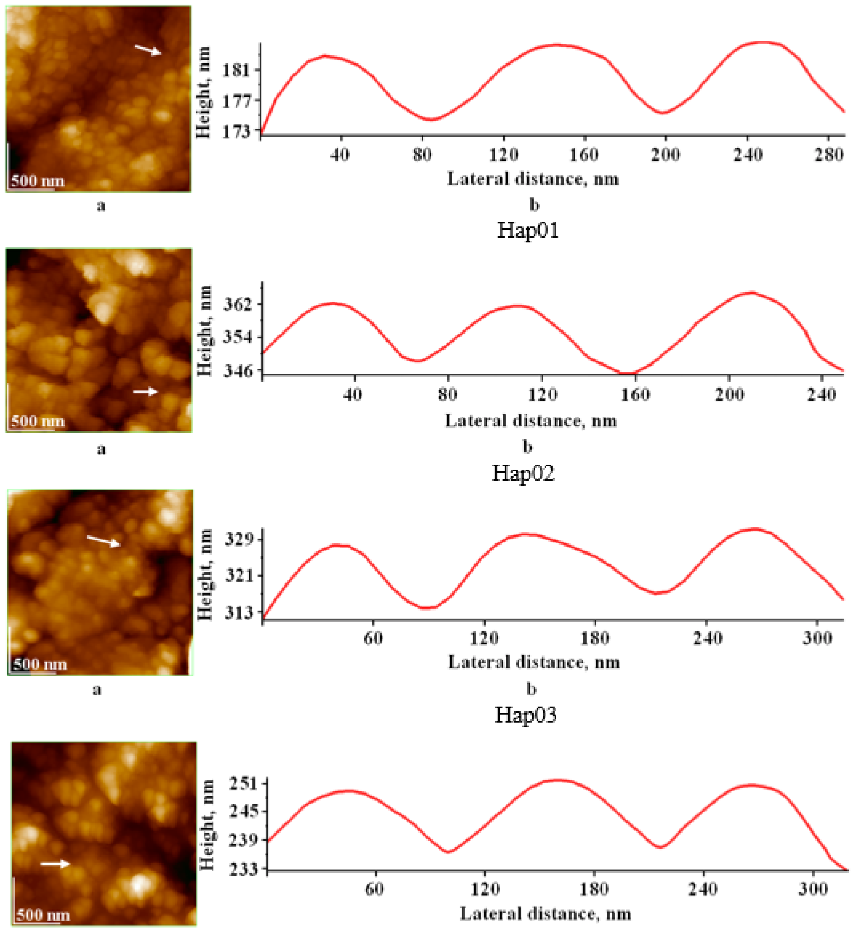

Fig. 5. AFM images for Hap01-Hap04, calcined at 650 °C, nanoparticles adsorbed on glass for 15 s from aqueous dispersion: (a) 2D-topography; (b) cross section profile along the arrow in image (a); scanned area: 2 x 2 µm; average particle size / root mean square: RMS on profile: 50 ± 4 nm / 3.2 nm (Hap01); 47 ± 5 nm / 6.3 nm (Hap02); 63 ± 6 nm / 5.3 nm (Hap03); 66 ± 6 nm / 4.4 nm (Hap04)

almost corresponding to synthesis (table 1). Additionally, Si was identified in Hap02 and Hap03, while Zn was identified in Hap04 (fig. 4). Si content in Hap04 was not identified being at a very low amount (table 1), probably under detection limit of EDX technique. In general, EDX mapping indicated that Mg was rather uniformly dispersed in all doped Hap powders. The EDX analysis agrees well with the chemical composition corresponding to the synthesis

Atomic force microscopy

AFM images and cross section profiles are given in figure 5 for doped Hap, Hap01-Hap04, calcined at 650°C.

The size of particles is found in the range from 47 nm to 66 nm for all doped Hap powders (table 1), showing only small variations. These values are comparable with those determined from specific surface area: SSA (BET measurements, table 3). As an example, the BET particle diameter, D_{BET}, of about 36 nm was estimated for Hap01, assuming the particles like spheres, using the formula: $D_{BET} = 6/(d \times SSA)$, where d is the theoretical density (3.156 g/cm^3) for hydroxyapatite [17], and used for all calculations. The nanostructure for all doped Hap powders, calcined at 650 °C, is also supported by SEM and XRD data. Thus, the nanostructure is preserved for all doped Hap powders, calcined at high temperature of 650 °C, having a high thermal stability.

Conclusions

Four doped Hap powders with different content of magnesium, zinc and silicon (table 1) were prepared by wet precipitation method, dried by lyophilisation, and then exposed to a thermal treatment process at 400, 650 or 850°C, each for 2h. The obtained powders were investigated by thermal analysis, BET measurements, XRD, SEM, SEM-EDX and AFM techniques. The nanostructure processing allowed a rather good control of the chemical composition of doped Hap, Hap01-Hap04 (table 1), as judged by SEM-EDX. The incorporation of various contents of Mg, Zn and Si in Hap lattice caused a distinctive different surface hydration of nanoparticles reflected in a characteristic modification of their thermal behaviour. Moreover, these results prove that dopant elements play a crucial role in enhancing the thermal stability of doped Hap powders. For instance, by calcination at 1000°C, their residue (wt%) was found to higher values with respect to those corresponding to stoichiometric pure Hap (table 2). Generally, the specific surface areas and porosity for all doped Hap powders decreased with increasing of calcination temperatures, as revealed by BET analysis (table 3). Thus, the calcination temperatures influence the size of nanoparticles and their surface properties. The effects of calcination temperature on particle size and morphology were determined by SEM and AFM imaging. It is observed that, the higher is the calcination temperature, the larger particle size is evidenced.

Certainly, multi-substituted Hap powders, with cations, such as Mg^{2+} and Zn^{2+}, and anions, such as SiO_4^{4-}, are closer to the biological hydroxyapatite than pure stoichiometric Hap. Consequently, multi-substituted Hap powders are promising nanoceramics for bone substitutes, as coating layers on metallic implants and carriers for drug delivery systems.

Acknowledgments: We acknowledge the Executive Agency for Higher Education, Research, Development and Innovation Funding (UEFISCDI) for financial support through the scientific research projects no. 171 and 241.

References

1. DOREMUS, R.H., J. Mater. Sci., **27**, nr.2, 1992, p. 285.

2. OH, S., OH, N., APPLEFORD, M., ONG, J.L., Am. J. Biochem. Biotechnol., **2,** nr.2, 2006, p. 49.

3. JITARU, S., HODISAN, I., TIMIS, L., LUCIAN, A., BUD, M., Clujul Medical, 2016, DOI: 10.15386/cjmed-612.

4. CHAUDHRY, A.A., KNOWLES, J.C., REHMAN, I., DARR, J.A., J. Biomater. Appl., **28**, nr.3, 2013, p.448.

5. QIU, Z.Y., NOH, I.S., ZHANG, S.M., Front. Mater. Sci., **7**, nr.1, 2013, p.40.

6. TOMOAIA, G., MOCANU, A., VIDA-SIMITI, I., JUMATE, N., BOBOS, L.D., SORITAU, O., TOMOAIA-COTISEL, M., Mater. Sci. Eng. C, **37**, nr.1, 2014, p.37.

7. KHAN, A.F., SALEEM, M., AFZAL, A., ALI, A., KHAN, A., KHAN, A.R., Mater. Sci. Eng. C, **35**, nr.1, 2014, p.245.

8. ARCOS, D., GREENSPAN, D.C., VALLET-REGI, M., J. Biomed. Mater. Res. A, **65**, nr.3, 2003, p.344.

9. ARCOS, D., VALLET-REGI, M., Acta Biomater., **6**, nr.8, 2010, p. 2874.

10. KOLMAS, J., JAKLEWICZ, A., ZIMA, A., BUCKO, M., PASZKIEWICZ, Z., LIS, J., SLOSARCZYK, A., KOLODZIEJSKI, W., J. Mol. Struct., **987,** nr.1-3**,** 2011, p.40.

11. LAURENCIN, D., ALMORA-BARRIOS, N., DE LEEUW, N.H., GERVAIS, C., BONHOMME, C., MAURI, F., CHRZANOWSKI, W., KNOWLES, J.C., NEWPORT, R.J., WONG, A., GAN, Z., SMITH, M.E., Biomaterials, **32**, nr.7, 2011, p.1826.

12. FARZADI, A., BAKHSHI, F., SOLATI-HASHJIN, M., ASADI-EYDIVAND, M., ABU OSMAN, N.A.., Ceram. Internat., **40**, nr.4, 2014, p.6021.

13. SADER, M.S., LEGEROS, R.Z., SOARES, G.A., J. Mater. Sci.: Mater. Med., **20**, nr.2, 2009, p.521.

14. LANDI, E., LOGROSCINO, G., PROIETTI, L., TAMPIERI, A., SANDRI, M., SPRIO, S., J. Mater. Sci.: Mater. Med., **19**, nr.1, 2008, p.239.

15. QI, G., ZHANG, S., KHOR, K.A., LYE, S.W., ZENG, X., WENG, W., LIU, C., VENKATRAMAN, S.S., MA, L.L., Appl. Surf. Sci., **255**, nr.2, 2008, p.304.

16. CACCIOTTI, I., BIANCO, A., LOMBARDI, M., MONTANARO, L., J. Eur. Ceram. Soc., **29**, nr.14, 2009, p.2969.

17. STIPNIECE, L., SALMA-ANCANE, K., BORODAJENKO, N., SOKOLOVA, M., JAKOVLEVS, D., BERZINA-CIMDINA, L., Ceram. Int., **40**, nr.2, 2014, p. 3261.

18. KANNAN, S., VENTURA, J.M., FERREIRA, J.M.F., Ceram. Int., **33**, nr.4, 2007, p.637.

19. ZIANI, S., MESKI, S., KHIREDDINE, H., Int. J. Appl. Ceram. Technol., **11,** nr**.** 1, 2014, p. 83.

20. GOZALIAN, A., BEHNAMGHADER, A., DALIRI, M., MOSHKFOROUSH, A., Sci. Iran., Trans. F, **18,** nr.6**,** 2011, p.1614.

21. RYU, H.S., HONG, K.S., LEE, J.K., KIM, D.J., J. Mater. Res., **21,** nr.2, 2006, p.428.

22. MISHRA, V.K., BHATTACHARJEE, B.N., PARKASH, O., KUMAR, D., RAI, S.B., J. Alloys Compd., **614**, 2014, p.283.

23. FERNANDEZ, M.E., ANGELES-CHAVEZ, C., MONDRAGON-GALICIA, G., RODRIGUEZ-LUGO, V., J. Mater. Sci..: Mater. Med., **15**, nr.6, 2004, p.735

24. SHEPHERD, J.H., SHEPHERD, D.V., BEST, S.M., J. Mater. Sci.: Mater. Med., **23**, nr.10, 2012, p.2335.

25. AHMADI, T., MONSHI, A., MORTAZAVI, V., FATHI, M.H., SHARIFI, S., BENI, B.H., ABED, A.M., KHERADMANDFARD, M., SHARIFNABI, A., Ceram. Int., **40**, nr.6, 2014, p.8341.

26. TOMOAIA, G., SORITAU, O., TOMOAIA-COTISEL, M., POP, L.B., Pop, A., MOCANU, A., HOROVITZ, O., BOBOS, L.D., Powder Technol., **238**, 2013, p.99.

27. GARBO, C., SINDILARU, M., CARLEA, A., TOMOAIA, G., ALMASAN, V., PETEAN, I., MOCANU, A., HOROVITZ, O., TOMOAIA-COTISEL, M., Particul. Sci. Technol., 2015, DOI: 10.1080/02726351.2015.1121180.

28. BOANINI, E., GAZZANO, M., BIGI, A., Acta Biomater., **6**, nr. 6, 2010, p. 1882.

29. KOHUTOVA, A., HONCOVA, P., SVOBODA, L., BEZDICKA, P., MARIKOVA, M., J. Therm. Anal. Calorim., **108**, nr. 1, 2012, p.163.

30. MOCANU, A., FURTOS, G., RAPUNTEAN, S., HOROVITZ, O., FLORE, C., GARBO, C., DANISTEANU, A., RAPUNTEAN, G., PREJMEREAN, C., TOMOAIA-COTISEL, M., Appl. Surf. Sci., **298**, 2014, p. 225.

31. TOMOAIA, G., POP, L.B., PETEAN, I., TOMOAIA-COTISEL, M., Mat. Plast., **49**, no. 1, 2012, p. 48.

32. TOMOAIA, G., TOMOAIA-COTISEL, M., POP, L.B., POP, A., HOROVITZ, O., MOCANU, A., JUMATE, N., BOBOS, L.D., Rev. Roum. Chim., **56**, nr. 10-11, 2011, p. 1039.

33. TOMOAIA, G., TOMOAIA-COTISEL, M., POP, L.B, MOCANU, A., POP, A., Romania, Patent nr.125817, BOPI, nr. 6, 2013, p. 123.

34. SPRIO, S., TAMPIERI, A., LANDI, E., SANDRI, M., MARTORANA, S., CELOTTI, G., LOGROSCINO, G., Mater. Sci. Eng. C, **28**, nr. 1, 2008, p. 179.

35. DOROZHKIN, S.V., EPPLE, M., Angew. Chem. Int. Ed.,, **41**, nr. 17, 2002, p. 3130.

36. COX, S.C., JAMSHIDI, P., GROVER, L.M., MALLICK, K.K., Mater. Sci. Eng. C, **35**, 2014, p. 106

37. BOGATU, L., DRAGOMIR, R., Rev. Chim. (Bucharest), **66**, no. 5, 2015, p. 722.

38. BOGATU, L., Rev. Chim. (Bucharest), **65**, no. 10, 2014, p.1230.

39. DINOIU, V., FLORESCU, D., BOGATU, L., Rev. Chim. (Bucharest), **58**, no. 2, 2007, p. 183.

40. HOROVITZ, O., TOMOAIA, G., MOCANU, A., YUPSANIS, T., TOMOAIA-COTISEL, M., Gold Bull., **40**, nr. 4, 2007, p. 295.

41. TOMOAIA, G., FRANGOPOL, P.T., HOROVITZ, O., BOBOS, L.D., MOCANU, A., TOMOAIA-COTISEL, M., J. Nanosci. Nanotechnol., **11**, nr. 9, 2011, p. 7762.

42. SPAGNOLI, D., ALLEN, J.P., PARKER, S.C., Langmuir, **27**, nr. 5, 2011, p. 1821.

Manuscris received: 23.09.2016